Proceedings of the 5th WSEAS/IASME Int. Conf. on SYSTEMS THEORY and SCIENTIFIC COMPUTATION, Malta, September 15-17, 2005 (pp108-113)

Numerical and Experimental analysis of long range guided waves for NonDestructiveTesting of pipes.

F. BERTONCINI, M. RAUGI
Department of Electric Systems and Automation
University of Pisa
Via Diotisalvi 56126 Pisa,
ITALY

Abstract: - In this paper numerical and experimental analysis of long range guided waves for non destructive testing of pipes is carried out. Guided waves based NonDestructiveTesting (NDT) methods offer considerable advantages over conventional techniques because they allow the inspection of wide areas from a single point of measure; therefore they are currently being investigated by some researchers. The analysis of the measured data from guided wave propagation in pipes requires advanced processing data systems to extract the right information on defect size and location. Then, a full comprehension of the physical phenomena underlying this technique is fundamental for a successful and reliable use of this technique. Then combined numerical and experimental analyses are of fundamental importance. In this paper a finite element code is used to numerical simulate the guided wave phenomenon in pipes. Furthermore, an experimental set-up showing critical characteristics has been arranged for the testing of the numerical data.

Key-Words: - Guided waves, numerical simulation, experimental analysis

1 Introduction

In general numerical modelling of ultrasound can be used as a flexible tool for examining the generation, propagation and interaction of elastic waves in solid materials for nondestructive evaluation (NDE), and they can be also used in order to build the database required for defect classification and sizing. Finite element models have been developed that demonstrate qualitative [1] agreement with experimental measurements and quantitative [2] agreement with an analytical half-space line source model. In both cases, the numerical code solves for transient displacement fields in linear, isotropic, twodimensional plane strain media.

The physical effect of anisotropy is included by specifying the material dependent elastic constants in the generalized stress-strain relationship known as Hooke's law. However, ultrasonic attenuation mechanisms are more difficult to incorporate in a numerical code since they are not only due to energy losses such as grain scattering and absorption or dissipation but also result from beam spreading of the elastic fields in the material [3]. Each of these mechanisms has been studied analytically and experimentally in the past.

Scattering is caused by a re-orientation and mode conversion of acoustic energy at microstructural interfaces and plays a major damping role in materials far which microstructural dimensions and interrogation wavelength are of the same order [4]. Efforts have also been made to develop a generalized scattering model but the task is complicated by the number of parameters involved in the description of the attenuation characteristics of a given polycrystalline material [5].

Energy absorption, the second major attenuation mechanism, is primarily characterized by irreversible thermal processes [6]. A major contributing factor, for example, is thermoelastic attenuation due to conduction between alternating compression and rarefaction regions in the elastic waves. Modelling and measuring work on energy absorption can be found in recent publications [7].

The numerical models [8], [9] are suitable for incorporating inhomogeneity, anisotropy and complex geometries, but they all suffer from the two-dimensional (2-D) nature of the code. The results, therefore, are not general enough to be useful far quantitative experimental verification studies. In a three-dimensional (3-D) code, the geometric factor is implicitly accounted for as part of the formulation , some theoretical and experimental results using FEM [10] [11], BEM [12], [13] have been presented and also FEM-BEM coupled schemes have been proposed [14].

In this paper we have used the code CAPA, based on the formulation showed in [14] to investigate the guided wave propagation phenomenon for several defect geometries. The most significant results will be shown together with a critical test comparing numerical and experimental data measured on a set-up arranged on a practical dismounted pipe for gas transportation.

2 Numerical analysis

Propagation and scattering of torsional elastic waves in a pipe with notch have been investigated varying the geometrical parameters of defect.

The test geometry is shown in Fig. 1. The defect region, located in $z=z_{d0}=1.3$ m, $\theta_{d0}=0°$, is characterized by the axial length Δz_d, the circumferential extent $\Delta\theta_d$ and the thickness parameter $t_d=(R_b-R_d)/(R_b-R_a)$ where R_a is the pipe internal radius R_a whereas R_d, R_b are the external radius in the region with and without defect respectively.

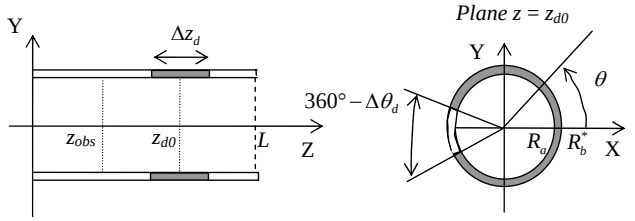

Fig. 1 – Geometry.

A transient numerical analysis has been carried out using CAPA, commercial software developed by WisSoft, Buckenhof, Germany. CAPA is a Finite-Element-Boundary-Element program for the numerical solution of coupled field problems in mechanical, electric, magnetic and acoustic domain.

A full 3D finite element analysis has been applied [15] on L=2.1 m long ideal steel pipe (ρ=7850 kg/m^3, E=2.157·10^{11} N/m^2, ν=0.3) with an 86 mm outside diameter and 5.5 mm thick wall. The pipe defect is located at $z=z_{d0}=1.3$ m plane.

The T(0,1) fundamental torsional mode is excited in the pipe by prescribing the circumferential displacements on the 36 external nodes belonging to z=0 plane. A tone burst excitation consisting of $N_h=6$ cycles at $f_0=55$ kHz modulated by an Hanning window is applied; its time length is $T_l=0.11$ms.

The incident and the reflected waves have been observed on the N=36 nodes P_n located in $z=z_{obs}=0.9$ m plane, uniform distributed along the exterior circumference and identified by the angle $\theta_n=(n-1)10°$, n=1, 2, …36.

The torsional component of the displacement

$$u_t(P_n, t)= -\sin(\theta_n)\cdot u_x(P_n, t) + \cos(\theta_n)\cdot u_y(P_n, t), \quad (1)$$

where u_x, u_y denote the Cartesian components, and its averaged value

$$u_{ta}(t)=\Sigma_n\, u_t(P_n, t)/N \quad (2)$$

are the most significant values of the displacement.

Preliminary tests have verified that only the T(0,1) non-dispersive mode propagates along the pipe with the theoretical group velocity c_T=3250 m/s. Therefore the wavelength is $\lambda= c_T \cdot f_0 \cong 60$ mm and the size of the smallest defect that can be identified (spatial resolution) is $l_{sr}= c_T\cdot T_l/2=\lambda N_h/2= 180$ mm.

Finally small and large defects in axial, circumferential and radial extent have been considered in axisymmetric and non axisymmetric configuration. The numerical results are presented and discussed below.

2.1 Scattering from axisymmetric defects

Axisymmetric defects ($\Delta\theta_d=360°$) have been considered with the following axial and radial extents:

Δz_d=3,60,210mm ≅0.05λ,λ,3.5λ; t_d=n·10%,n=1,2,..,9 (3)

In the results the radial and axial components of displacement are null. As expected, with an incident torsional wave the reflected and transmitted waves are torsional too.

Fig. 2a shows the incident wave $x_{inc}(t)$ whereas the variation of reflected signal $y_{refl}(t; t_d)$ with defect depth t_d when Δz_d=3mm is shown in Fig. 2b. The incident pulse can be weakly or strongly attenuated from the defect but its shape doesn't change as the Fast Fourier Transformation of incident and reflected signals confirms (see Fig. 3). The reflection coefficient (computed as $R(t_d; f_0)=|Y_{refl}(f_0; t_d)|/ |X_{inc}(f_0)|$) has been compared with values computed and measured in [16]; the agreement shown in Fig. 4 is good.

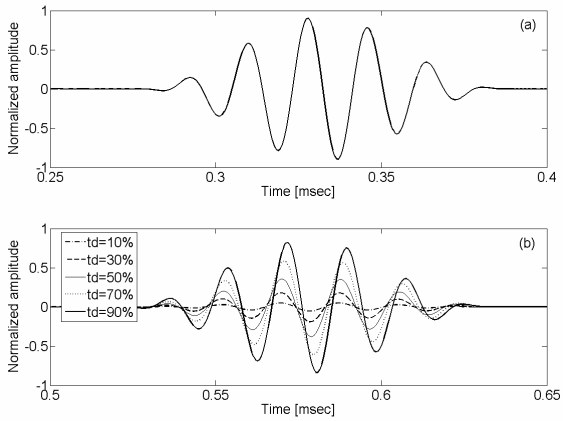

Fig. 2 – (a) Incident wave and (b) reflected wave vs. defect depth (Δz_d=3mm).

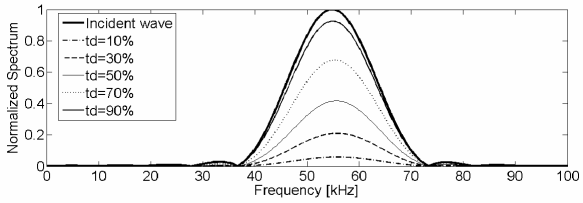

Fig. 3 – Spectrum of the incident and the reflected waves vs. defect depth (Δz_d=3mm).

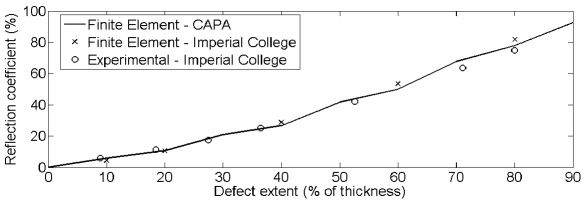

Fig. 4 –Reflection ratio vs. defect depth (Δz_d=3mm).

The effect of the defect axial extent is shown in Fig. 5 when t_d=50%. If Δz_d is very small respect to the spatial resolution l_{sr} (see Fig. 5a) there isn't distortion in the reflected signal but only attenuation with respect to the incident signal. Otherwise when Δz_d is comparable to l_{sr}, the reflected signal from defect is the result of the interaction between two distinct geometric discontinuities: the stepwise thickness located in $z_A=z_{0d}-\Delta z_d/2$ (discontinuity A) and that other one located in $z_B=z_{0d}+\Delta z_d/2$ (discontinuity B). This is evident in Fig. 5c where $\Delta z_d > l_{sr}$: in the reflected signal there are four distinct pulses related to the reflection from A and to the single, double and triply interaction between A and B.

For the first pulse the theoretical arrival time and the reflection coefficient are

$$t_A=[z_A+(z_A-z_{obs})]/c_T = 0.46 \text{ ms}, \quad (4)$$

$$R_A=(Z_2-Z_1)/(Z_2+Z_1)=(A_2-A_1)/(A_2+A_1)=-0.35 \quad (5)$$

rispectively.

In (4) the acoustic impedance $Z_i=\rho c_T A_i$ and the cross-sectional area of the pipe A_i are evaluated [17], [18] in the section 1 ($z<z_A$) for the incident wave and in the section 2 ($z>z_A$) for the transmitted wave.

For the interaction between A, B it is:

$$t_n= t_A+n\cdot 2\Delta z_d/c_T= 0.59, 0.72, 0.85 \text{ ms}, \quad (6)$$

$$R_n=(1+R_A)(-R_A)^{2n-1}(1-R_A)=0.31, 0.04, 0.005 \quad (7)$$

where n=1, 2, 3 for the single, doubly and triply interaction respectively.

The numerical results shown in Fig. 5c agree with these theoretical values.

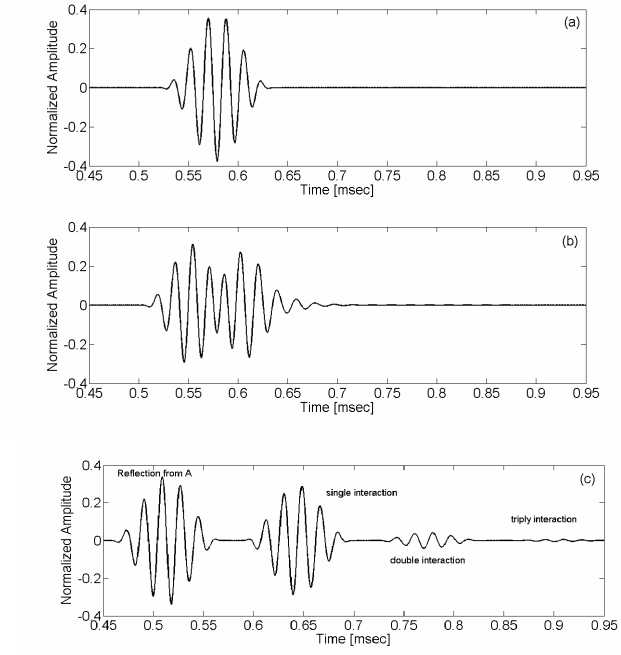

Fig. 5 –Reflected signal vs. axial length: t_d=50%, (a) Δz_d=3 mm, (b) Δz_d=60 mm, (c) Δz_d=210 mm.

2.2 Reflection from non-axisymmetric defect

The reflection of the incident T(0,1) mode from non-axisymmetric defect has been investigated using the following values for defect parameters (see Fig. 1):

t_d=10, 30, 50, 70, 90 %;

$\Delta\theta_d$=10, 20, 30, 40 °; (8)

Δz_d=3, 6, 12, 18, 24 mm= 0.05λ, 0.1λ, 0.2λ, 0.3λ, 0.4λ.

The results of the 3D analysis show that the non-axisymmetric defect not only excites the torsional mode but the longitudinal and flexural modes too. As shown in Fig. 6a, related to the case t_d=50%, $\Delta\theta_d$=30°, Δz_d=12 mm, the radial and axial component of the displacement can be comparable with the circumferential component when the reflected wave is evaluated in a single point.

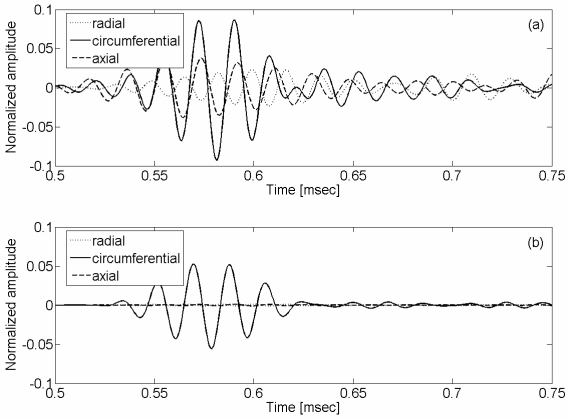

Fig. 6 – Cylindrical components of the displacement: (a) single point x_P= y_P=30.4mm, z_P=0.9m and (b) averaged values.

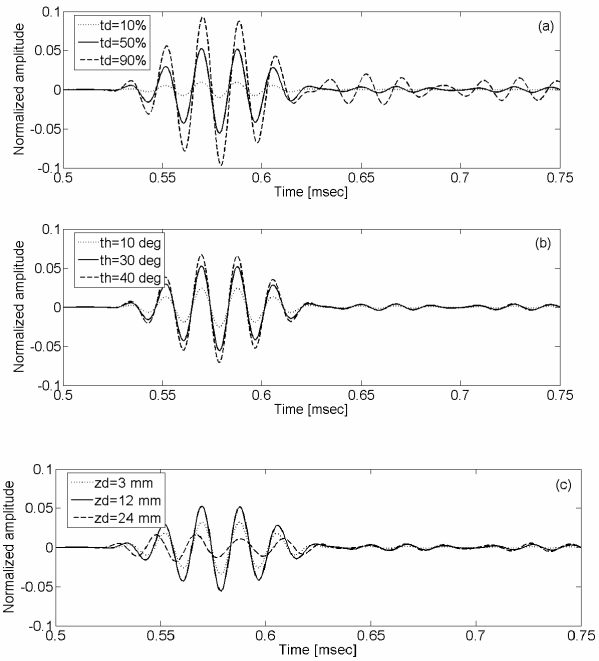

Fig. 7 –Reflected signal vs. (a) defect depth, (b) circumferential length, (c) axial length. Averaged values of the circumferential displacement component.

Nevertheless, if the average displacement is computed along the circumference the circumferential component is dominant (see Fig. 6b). Some significant results for the circumferential component (averaged values) are shown in Fig 7a, b, c where one of the three parameters t_d, $\Delta\theta_d$, Δz_d changes with respect to the reference values t_d=50%, $\Delta\theta_d$=20°, Δz_d=12 mm.
The reflected signal sensitivity with respect to the geometrical parameters of the defect seems very strong.

3 Experimental results

Experimental data have been obtained using a dismounted steel pipe for gas transportation. The sample was 3.4 m long with 114 mm outside diameter and 8.3 mm thick. The reflection from a patch (circumferential and axial length 0.19 m and 0.43 m respectively, thickness 10 mm) arranged to repair the pipe has been investigated using MsSR – 2020 D instrument. The instrument, developed by SwRI South West Research Institute in San Antonio, Texas, is based on magnetostrictive sensor technology: by using appropriate probes it is able to generate and detect guided wave up to 250 kHz in pipes, plates, rods and cables [19].
The instrument has been arranged in pitch-catch configuration as shown in Fig. 8 to generate (TX probe) and detect (RX probe) torsional waves in the pipe under test. The distance between the two probes was z_{TR}=0.4m and measured data have been obtained exciting in the pipe 1 cycle pulse of 64 kHz.

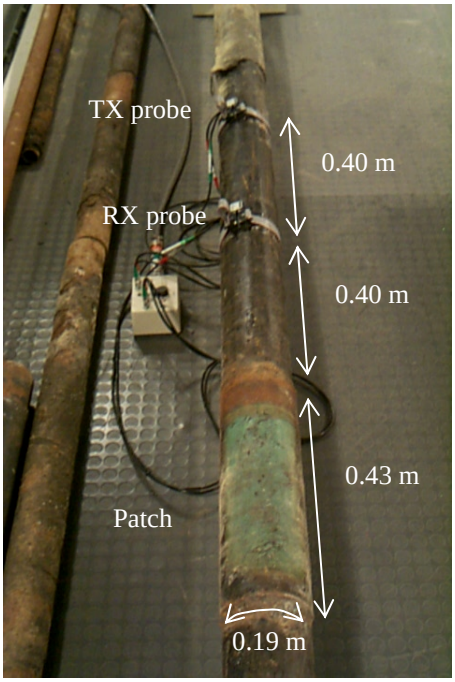

Fig. 8 - Experimental setup.

Initially the shear wave velocity c_T =3240 m/s has been calculated by using the signals in the measured data related to known geometric features. In the sample the distance between the probes and the ends of pipe is known. Then the measured data related to the reflection from the patch have been acquired as Fig. 9 shows. In the figure the initial pulse and the reflected pulses from the patch can be recognized. As a matter of fact the reflected pulses are related to the pipe wall thickness change at z_A = 0.4 m and z_B = 0.83 m distance from the RX probe. The theoretical arrival times

$$t_A = (z_{TR} + 2\cdot z_A)/c_T = 0.37 \text{ msec}, \quad (9)$$

$$t_B = (z_{TR} + 2\cdot z_B)/c_T = 0.63 \text{ msec}, \quad (10)$$

agree with the experimental results shown in Fig. 9.
In particular not only the geometrical discontinuities in the pipe are recognized but also the axial extent of the patch can be computed from measured data. It is

$$\Delta z_d = c_T\cdot(t_B - t_A)/2 = 0.42 \text{ m}, \quad (11)$$

with good agreement with the real axial extent.

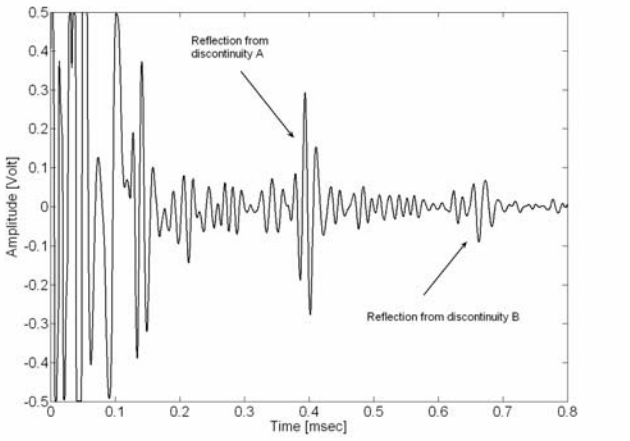

Fig. 9 – Torsional measured component of the displacement.

4 Combined numerical and experimental analyses

A combined numerical and experimental analysis has been carried out using the test sample described in the previous section. The aim was to investigate how the right information on defect size and location can be extracted from measured/computed data.
A finite element analysis of the dismounted pipe shown in Fig. 8 has been executed using the code CAPA. In particular the patch has been modelled as stepwise thickness change without the welds existing in the real pipe. Moreover in the model the circumferential location and extent of the patch was (see Fig. 1) θ_{d0}=0°, $\Delta\theta_d$=220° respectively. Finally a torsional excitation of 64 kHz has been applied and the reflected signal from the patch has been observed in 36 circumferential nodes at 0.4 m distance from the patch itself.
Fig. 10 shows the averaged value of the circumferential component of the displacement. This figure can be compared with the experimental results shown in Fig. 9. In particular, the amplitude of the reflections from A and B have the same ratio both in fig. 9 and 10.

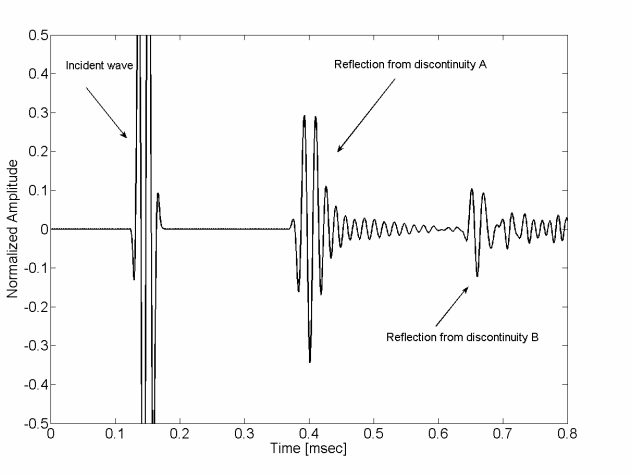

Fig. 10 – Torsional computed component of the displacement

The qualitative agreement between numerical and measured results is good confirming that the averaged value of the torsional component of displacement is able to detect the axial discontinuities in the pipe and the axial extent of the defect. Nevertheless this analysis is possible because the defect is known. In general the only torsional component of the displacement can be used to detect the defect but it is not sufficient to identify and to size the defects. As shown in the section 2 the torsional component is sensitivity with respect to the axial, circumferential and radial extent of the defect. So other displacement variables are needed to identify and to size a defect. In the following the circumferential extent of a strip is investigated by the numerical analysis with code CAPA. The strip is a geometrical simplification of the patch used above to simulate the pipe shown in Fig. 8. In particular the strip can be view as a patch with infinite axial length. So in the reflected signal shown in Fig. 11 there is only one pulse; in particular the reflection from the patch and the strip coincide until $t<t_B$ where the time t_B (see (6)) is related to the reflection from the second discontinuity z_B in the patch.

The effect of the defect circumferential extent has been analysed with the following values $\Delta\theta_d$=120, 220, 320, 360 °.

Initially, the averaged value of the torsional component of the displacement has been evaluated. As already known (see Fig. 7b) and as shown in Fig. 12 the amplitude of this component increases when $\Delta\theta_d$ increases.

Then the new displacement variable

$$u_{fa}(t\,;\Delta\theta_d,\theta_0)=\Sigma_n\,[u_t(P_n,t\,;\Delta\theta_d)\cdot\cos(\theta_n-\theta_0)]/N \qquad (12)$$

has been defined.

This variable is connected [19] to the circumferential component of displacement in a flexural wave.

At first u_{fa} has been evaluated with $\Delta\theta_d$=220° and $\theta_0=(n-1)\cdot 30°$, n =1, 2, …12. The amplitude $|u_{fa}(t\,;220°,\theta_0)|$ is maximum when θ_0=0, 180°: those values are related to symmetry plane of the defect (see Fig. 1).

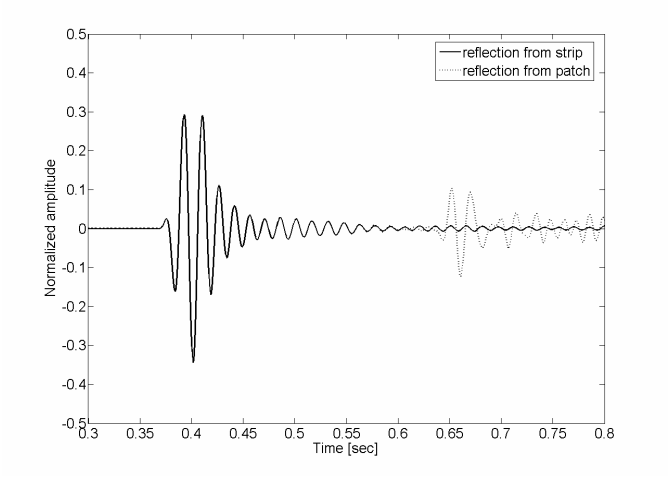

Fig. 11 – Torsional computed component of the displacement for the strip (solid line) and for the patch (dashed line).

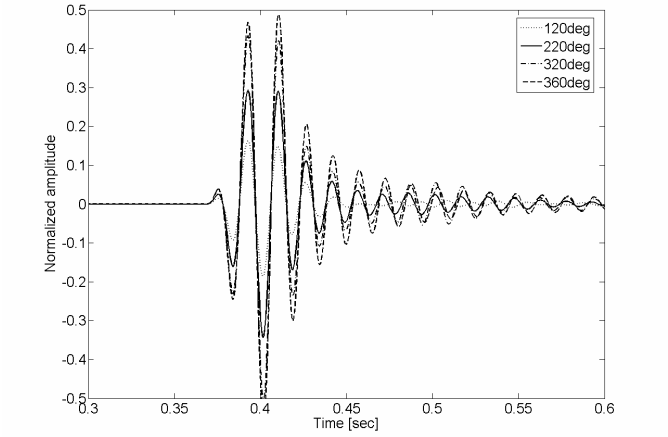

Fig. 12 – Torsional computed component of the displacement for the strip.

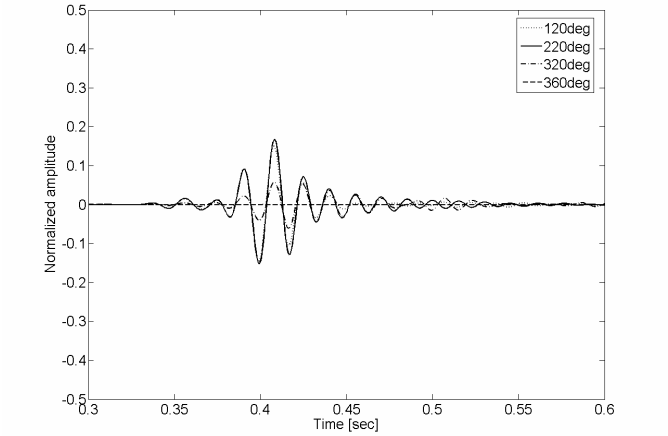

Fig. 13 – Computed component u_{fa} of the displacement for the strip.

Subsequently u_{fa} has been evaluated with $\Delta\theta_d$=120, 220, 320, 360° and $\theta_0=\theta_{d0}$=0°. The results are shown in Fig. 13: when $\Delta\theta_d$ increases from 220° to 360° the amplitude

of u_{fa} decreases; in particular u_{fa} is null with $\Delta\theta_d=360°$ that is when the defect is axisymmetric.
Therefore the variable u_{fa} seems useful not only to size the circumferential extent of the defect but also to locate the defect on the pipe circumference.

5 Conclusion

A combined numerical and experimental analysis of non-destructive testing of pipes by Ultrasonic guided waves had been carried out. Numerical results had been validated with computed and measured data available in the literature and tested with an experimental set-up arranged on a practical dismounted pipe for gas transportation. A suitable combined numerical and experimental analysis carried out by defining an appropriate displacement variable has given appropriate information to detect size and location of a defect.

5 Acknowledgements

This work was supported in part by the Ministry of University under a Program for the Development of Research of National Interest PRIN 2003094558.
We thank ToscanaGas SpA for providing dismounted pipes.

References:

[1] R. Ludwig and W. Lord, "A finite element formulation far the study of ultrasonic NDT systems," IEEE Trans. Ultrason. Ferroelec. Freq. Contr., voI. 35, pp. 809-820, 1988.
[2] R. Ludwig, D. Moore and W. Lord, "An analytical and numerical study of transient force excitations on an elastic halfspace," IEEE Trans Ultrason. Ferroelec. Freq. Contr., voI. 36, pp. 342-350, 1989.
[3] R. L. Roderick and R. Truell, "The measurement of ultrasonic attenuation in solid by the pulse technique and some results in steel," J. Appl. Phys., vol. 23, no. 2, pp. 267-279, 1952.
[4] E. P. Papadakis, "Ultrasonic attenuation caused by scattering in polycrystalline metals," J. Acoust. Soc. Amer., voI. 37, no. 4, pp. 711-717, 1965.
[5] S. Serabian and R. S. Williams, "Experimental determination of ultrasonic attenuation characteristics using the Roney generalized theory," Materials Evaluation, vol. 36, no. 1, pp. 55-62, 1978.
[6] W. P. Mason, Physical Acoustics and the Properties of Solids, Princeton, NJ: Van Nostrand, 1958.
[7] R. Lerch and W. Friedrich, "Ultrasonic fields in attenuating media," J. Acoust. Soc. Amer., vol. 80, no. 4, pp. 1140-1147. 1986.
[8] K. J. Langenberg et al., "Numerical modelling of ultrasonic scattering," in Mathematical Modelling in Nondestructive Testing, M. Blakemore, G. A. Georgiou, Eds. Oxford, UK: Clarendon Press, 1988, pp. 125-173.
[9] L. J. Bond, M. Punjani and N. Saffari, "Ultrasonic wave propagation and scattering using explicit finite difference methods." Mathematical Modelling in Nondestructive Testing, M. Blakemore, G. A. Georgiou Eds. Oxford, UK: Clarendon Press, 1988, pp. 81-124.
[10] R. Lerch, "Simulation of piezoelectric devices by two- and three-dimensional finite elements", IEEE Trans on Ultrasonics Ferr. and Freq. Vol 37 n.2 May 1990, pp 233-247,
[11] M. Koshiba, K. Hasegawa, and M. Suzuki, "Finite-element solution of horizontally polarized shear wave scattering in an elastic plate", IEEE Trans. Ultrason. Ferroelec. Freq. Contr., vol. 34, no. 4, pp. 461-466, 1987.
[12] Y. Cho, J. L. Rose, A boundary element solution for a mode conversion study on the edge reflection, JASA, vol. 99, no. 4, pt. 1, pp. 2097-2109
[13] S. P. Pelts, J. P. Cysyk, J. L. Rose, The boundary element method for Flaw Classification in Wave Guides, Review of Progress in Quantitative Nondestructive Evaluation, vol. 16, Plenum Press, New York, pp. 137-143, 1996.
[14] M. Kaltenbacher, H. Landes, R. Lerch, "An efficient calculation scheme for the numerical simulation of coupled magnetomechanical systems" IEEE Trans. On Mag., Vol 33, n. 2, March 1997, pp1646-1649.
[15] M. Kaltenbacher, Numerical Simulation of Mechatronic Sensors and Actuators, Springer-Verlag Berlin Heidelberg, 2004.
[16] A. Demma, P. Cawley, M. Lowe, A. G. Roosenbrand, "The reflection of the fundamental torsional mode from cracks and notches in pipes" – J. Acoust. Soc. Am 114 (2), August 2003.
[17] M. S. Choi, S. Y. Kim, H. Kwun, G. M. Light, "Transmission line model for simulation of guided wave defect signals in piping", IEEE Trans. Ultrason. Ferroelectr. Freq. Control, vol. 51, pp. 640-643, 2004.
[18] H. Kwun,, S. Y. Kim, M. S. Choi, "Experimental comparison of analytical modelling of guided-wave interaction with a notch in a pipe", J. Korean Physical Soc., vol. 45, pp. 380-385, 2004.
[19] H. Kwun, S. Y. Kim, G. M. Light – "Long-Range Guided Wave Inspection of Structures Using the Magnetostrictive Sensor" – Applied Physics Division, Department of NDE Science and Technology, Southwest Research Institute, San Antonio, Texas, 78238 USA.
[20] J. D. Achenbach, Wave propagation in elastic solids, North Holland Publishing Company, 1975.